11th World Congress on Computational Mechanics (WCCM XI)
5th European Conference on Computational Mechanics (ECCM V)
6th European Conference on Computational Fluid Dynamics (ECFD VI)
E. Oñate, J. Oliver and A. Huerta (Eds)

NUMERICAL SIMULATION OF FREE SURFACE FLOWS, WITH MULTIPLE LIQUID PHASES

A. Caboussat[1], N. James[2], S. Boyaval[3] and M. Picasso[4]

[1] Geneva School of Business Administration, HES-SO//University of Applied Sciences, Western Switzerland, Route de Drize 7, 1227 Carouge, Switzerland, e-mail: alexandre.caboussat@hesge.ch, web page: http://campus.hesge.ch/caboussata

[2] Université de Poitiers, Lab. de Mathématiques, Futuroscope Chasseneuil Cedex, France, e-mail: nicolas.james@math.univ-poitiers.fr, web page: http://www-math.univ-poitiers.fr/∼njames/

[3] Université Paris Est, Laboratoire d'hydraulique Saint-Venant 78401 Chatou Cedex, France, e-mail: sebastien.boyaval@saint-venant.enpc.fr, web page: http://www.saint-venant-lab.fr/

[4] MATHICSE, Ecole Polytechnique Fédérale de Lausanne, Station 8, 1015 Lausanne, e-mail: marco.picasso@epfl.ch, web page: http//people.epfl.ch/marco.picasso

Key words: Multiphase flow, Free surfaces, Volume-of-fluid, Time splitting algorithm, Immiscible phases, Landslides.

Abstract. We present a numerical framework for the simulation of multiphase flows with free surfaces, thus considering N incompressible liquid phases together with a vacuum. An Eulerian model is favored to track the liquid phases, based on several characteristic functions. The numerical algorithm relies on a time splitting strategy, together with a two-grid discretization method. Numerical experiments are presented for impulse waves, and for rigid bodies falling into an incompressible liquid.

1 INTRODUCTION

We address the numerical simulation of three-dimensional multiphase flows with free surfaces. A model for several liquid phases interacting with one gas phase is presented. This model is an extension of the one described in [2, 9] and has been originally presented in [8]. Among all possible approaches (see, e.g., [12, 13]), an Eulerian approach is chosen to efficiently solve situations with large changes of topologies.

Thus we consider the density-dependent incompressible Navier-Stokes equations modeling the flow of N immiscible incompressible liquid phases separated by interfaces and one additional gas phase (modeled by a vacuum) separated from the liquids by a free surface. Such three-dimensional multi-phase flows involves thus a total of $N + 1$ phases.

A volume-of-fluid (VOF) formulation involving N indicator functions (one per phase, identified by its density) is favored for mass conservation. The governing equations of the model include the density-dependent Navier-Stokes equations for the velocity $\mathbf{u}$ and pressure p, together with N advection equations for the volume fractions φ_ℓ. The complete system of partial differential equations is solved by means of a flexible operator splitting strategy [6], which decouples advection and diffusion phenomena at each time step. A two-grid method allows to solve transport equations on a fine structured Cartesian grid, and a Stokes problem, with a variable density and a density-dependent viscosity, on a coarser mesh of the liquid domain. As also highlighted, e.g., in [1, 3, 4, 10], where several algorithms are described for interface reconstruction, a particular emphasis is paid on the numerical approximation of the interfaces between liquid phases and of the free surface between liquid and the gas phase.

Numerical experiments focus on the numerical simulation of impulse water waves created by landslides falling into a lake [11], and the interaction between a rigid body, modeled as a very viscous incompressible fluid, and an incompressible liquid. All these examples involve typically two liquid phases and a vacuum.

2 MATHEMATICAL MODEL

Consider Λ a bounded cavity of $\mathbb{R}^3$, that contains N immiscible liquids (with $N \geq 2$), whose densities and viscosities are respectively denoted by ρ_ℓ and μ_ℓ, $\ell = 1, \ldots, N$. It is assumed that the region in the cavity not occupied by liquid contains vacuum. For each phase ℓ, the subset of Λ occupied by the ℓ-th liquid is denoted by $\Omega_\ell(t)$, and defined by a characteristic function $\varphi_\ell : \Lambda \times [0, T) \to \mathbb{R}$. The function $\varphi := \sum_{\ell=1}^{N} \varphi_\ell$ is the characteristic function of the global liquid domain $\Omega(t) = \bigcup_{\ell=1}^{N} \Omega_\ell(t)$.

The model problem is to find $\mathbf{u} : \Omega(t) \to \mathbb{R}^3$, $p : \Omega(t) \to \mathbb{R}$, and $\varphi_\ell : \Lambda \to \mathbb{R}$ satisfying the following set of equations:

$$\rho \left(\frac{\partial \mathbf{u}}{\partial t} + (\mathbf{u} \cdot \nabla)\mathbf{u} \right) - \nabla \cdot (2\mu(\rho)\mathbf{D}(\mathbf{u})) + \nabla p = \rho \mathbf{f} \tag{1}$$

$$\nabla \cdot \mathbf{u} = 0\,, \tag{2}$$

$$\frac{\partial \varphi_\ell}{\partial t} + \mathbf{u} \cdot \nabla \varphi_\ell = 0\,, \quad \ell = 1 \ldots N\,, \tag{3}$$

where the density is expressed as $\rho = \sum_{\ell=1}^{N} \varphi_\ell \ \rho_\ell$ in the liquid space-time domain $\{(\mathbf{x}, t) \mid \mathbf{x} \in \Omega(t),\ t \in (0, T)\}$ ($\rho = \rho_\ell$ and $\mu = \mu_\ell$ in the region occupied by the ℓ-th liquid). We add appropriate initial and boundary conditions to the equations (1)–(3), namely no-slip or pure-slip boundary conditions along impermeable walls $\partial\Omega(t) \cap \partial\Lambda$. On the free surface $\Gamma(t) := \partial\Omega(t) \setminus \partial\Lambda$, we enforce a free force condition that reads $-p\mathbf{n} + 2\mu(\rho)\mathbf{D}(\mathbf{u})\mathbf{n} = 0$. Note that for the impulse waves applications we are interested in, surface tension effects can be negligible.

3 NUMERICAL ALGORITHMS

3.1 Generalities

The numerical method for the solution of (1)–(3) relies on an operator splitting algorithm for time discretization and a two-grid method for space discretization. The underlying principle in the time discretization is to decouple advection and diffusion operators, while taking a higher resolution when dealing with the interfaces reconstruction and approximation. This approach leads to a two-grid method (see Figure 1): the transport equations are solved on a fine structured Cartesian grid $\mathcal{C}_h$ of typical size h (to reduce numerical diffusion thanks to a small mesh size). On the other hand, the diffusion operators are solved on a coarse finite element mesh $\mathcal{T}_H$ of Λ of typical size H. Following [9], in numerical experiments the sizes of the two grids satisfy $H \simeq 5h$.

On one hand, the use of a fine Cartesian grid allows numerical diffusion, when solving the transport equations, to be reduced as much as possible. On the other hand, the use of a coarse finite element mesh allows the diffusion problem to be solved with sufficient accuracy and reasonable CPU time.

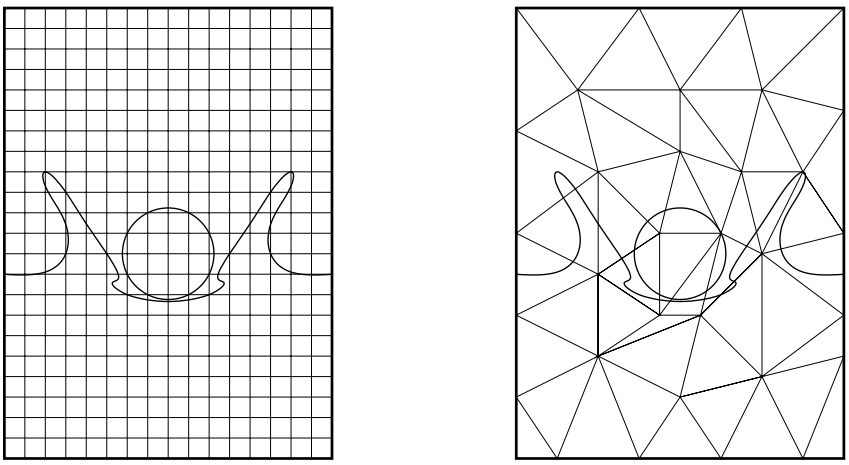

Figure 1: Illustration of the two-grids method in two space dimensions for liquid 1 (a rigid body in the limit case when the viscosity is large) falling onto liquid 2 (a flat water surface for instance): a Cartesian grid of structured cubic cells $\mathcal{C}_h$ of typical size h (left) is superimposed with a finite element unstructured tetrahedral mesh $\mathcal{T}_H$ of typical size H (right).

For $n \geq 0$, let $t^n = n\tau$ be a sequence of discrete times. Let Ω_ℓ^n and Ω^n be approximations of $\Omega_\ell(t^n)$ and $\Omega(t^n)$ respectively, defined by $\Omega^n = \{\mathbf{x} \in \Lambda : \varphi^n(\mathbf{x}) = 1\}$ and $\Omega_\ell^n = \{\mathbf{x} \in \Lambda : \varphi_\ell^n(\mathbf{x}) = 1\}$.

3.2 Advection operators

First, we solve the advection operators

$$\frac{\partial \mathbf{u}}{\partial t} + \mathbf{u} \cdot \nabla \mathbf{u} = 0\,, \qquad \frac{\partial \varphi_\ell}{\partial t} + \mathbf{u} \cdot \nabla \varphi_\ell = 0\,,\ \ \ell = 1 \dots N\,,$$

with a forward characteristics method:

$$\mathbf{u}^{n+1/2}(\mathbf{x} + \tau \mathbf{u}^n(\mathbf{x})) = \mathbf{u}^n(\mathbf{x}),\ \ \mathbf{x} \in \Omega^n, \tag{4}$$

$$\varphi_\ell^{n+1}(\mathbf{x} + \tau \mathbf{u}^n(\mathbf{x})) = \varphi_\ell^n(\mathbf{x}),\ \ \mathbf{x} \in \Omega_\ell^n\,,\ \ \ell = 1 \dots N. \tag{5}$$

It allows to obtain the new value of the volume fractions φ_ℓ^{n+1} (thus to define the new location Ω_ℓ^{n+1} of each liquid phase), and a predicted value of the liquid velocity $\mathbf{u}^{n+1/2}$ in Ω^{n+1}.

More precisely, the approximations φ_ℓ^n and $\mathbf{u}^n$ at time t^n at the center of each cell (ijk) of $\mathcal{C}_h$ are approximated by the piecewise constant values $(\varphi_\ell^n)_{ijk}$ and $\mathbf{u}_{ijk}^n$. These quantities are translated by $\tau \mathbf{u}_{ijk}^n$ on the time interval (t^n, t^{n+1}) along the straight line characteristics starting in the middle of each cell, and projected onto the fixed grid $\mathcal{C}_h$. This step defines new cell values $(\varphi_\ell^{n+1})_{ijk}$ and $\mathbf{u}_{ijk}^{n+1/2}$. The stability of this forward characteristics method is not restricted by any CFL condition, although accuracy is CFL dependent. A CFL number up to 5 is used in practice. Details can be found in [8, 9].

The drawbacks of the method include the projection error that spreads $(\varphi_\ell^n)_{ijk}$ onto all the cells overlapped by the transported cell (ijk) leading the numerical diffusion, and the compression error that comes from values of the volume fraction potentially greater than one in some cells. To reduce the numerical diffusion or the unphysical mixing of phases, we use a *multiphase* version of the SLIC algorithm [2, 9, 14]. On the other hand, a taylored DECOMPRESSION algorithm is used to reduce the compressibility effect and guarantee mass conservation. Both algorithms are described in details in [8] and briefly summarized in the next section.

3.3 Interface reconstruction

Maintaining the accuracy of each sharp interface between phases is important in the context of immiscible liquid flows to prevent numerical diffusion. There exist various ways of preventing the numerical diffusion of a transported characteristic function, see, e.g., [1, 3, 4, 12, 13]. Here, we use a SLIC algorithm *before* the advection step (4)(5) Whenever $(\varphi_\ell^n)_{ijk} \in (0, 1)$, the location of the liquid is condensed to a portion of the cell (ijk) with relative volume $(\varphi_\ell^n)_{ijk}$. The SLIC procedure has been chosen, over the PLIC procedure for instance, for its simplicity to be handled within the two-grid framework. The fact that SLIC is less accurate is compensated by working on a finer structured grid (for the advection only). We apply recursively the SLIC algorithm described in [14] for each of the liquid phases: we push the first liquid phase onto the sides or onto the corners of the cell before advecting it and projecting on the grid, then the second liquid phase, etc. Details can be found in [8].

After the interface reconstruction and advection steps, it may happen that some cell (ijk) in the grid $\mathcal{C}_h$ is over-filled, i.e. $\varphi_{ijk}^{n+1} = \sum_{\ell=1}^{N} (\varphi_\ell)_{ijk}^{n+1} > 1$. Such physically non-admissible values can indeed occur since the transport-and-project algorithm is not a divergence-free process. The DECOMPRESSION algorithm is a post-processing technique used in [9], which has been extended to multiple phases in [8]. The principle is in two steps: first, we compute the excess of each liquid phase in each cell after advection, second, we redistribute these amounts *proportionally to the amount already included in the cell* in a given arbitrary order. Details can be found in [8].

After the advection, approximations of the velocity $\mathbf{u}_H^{n+1/2}$ and volume fraction φ^{n+1} at t^{n+1} are numerically interpolated by continuous, piecewise linear functions on $\mathcal{T}_H$. An approximation Ω_H^{n+1} of the liquid domain can then be defined as the union of elements in $\mathcal{T}_H$ where φ_H^{n+1} is greater than $1/2$ at at least one vertex.

3.4 Diffusion operators

The final value of the liquid velocity $\mathbf{u}^{n+1}$ and pressure p^{n+1} in Ω^{n+1} at each time step is obtained via the solution of an implicit Stokes problem in Ω^{n+1}:

$$\rho^{n+1} \frac{\mathbf{u}^{n+1} - \mathbf{u}^{n+1/2}}{\tau} - 2\nabla \cdot \big(\mu(\rho^{n+1}) \mathbf{D}(\mathbf{u}^{n+1})\big) + \nabla p^{n+1} = \rho^{n+1} \mathbf{f}^{n+1}, \tag{6}$$

$$\nabla \cdot \mathbf{u}^{n+1} = 0, \tag{7}$$

where $\rho^{n+1} = \sum_{\ell=1}^{N} \varphi_\ell^{n+1} \, \rho_\ell$. The discretization of (6) (7) with a stabilized finite element (FE) discretization [5] is completed with suitable boundary conditions, at the boundary of a polyhedral approximation Ω_H^{n+1} of Ω^{n+1}. In particular, the density and viscosity are defined respectively by constant approximations ρ_H^{n+1} and μ_H^{n+1}, on each element of the mesh $\mathcal{T}_H$ by averaging the values at the vertices of the element.

4 NUMERICAL EXPERIMENTS

We present two types of numerical experiments. First the simulation of a landslide wave acts as a validation and benchmark example. Second the simulation of waves created by the fall of rigid bodies is discussed.

4.1 Landslide wave

The simulation of a landslide wave created by a granular slide on an inclined plane is presented. The landslide is modeled by a Newtonian fluid, with a large viscosity $\mu = 10^5$ [Pa s]. Following [7], we consider a bulk slide of dimensions $0.6 \times 0.118 \times 0.472$ [m^3] with density 1678 [kg m^{-3}], which slides on a 45 degree ramp that ends in a channel with 0.5 [m] width and 3.43 [m] length. The slide impact velocity value, $v = 4.67$ [$m\ s^{-1}$], is determined by the experimental process and used as initial condition of the numerical simulations, and the water depth is initially equal to 0.3 [m].

A probe is located in the channel at $x = 1.43$ [m] and is used to compare experimental and calculated results. Figure 2 shows snapshots of a three-dimensional view of the simulation. Figure 3 (left) illustrates the relative wave elevation versus the relative time and a comparison with experimental results. Figure 3 (right) illustrates the convergence when the discretization mesh size tends to zero (three discretizations with $(h = 0.005, H = 0.025, \tau = 0.02)$, $(h = 0.0025, H = 0.0167, \tau = 0.01)$, $(h = 0.0025, H = 0.0125, \tau = 0.005)$, have been considered).

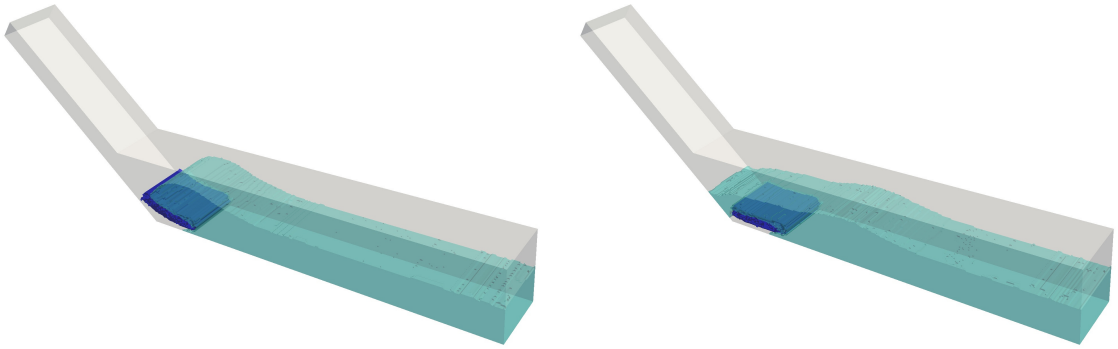

Figure 2: Wave generated by a landslide; snapshots of the simulation at times $t = 4$ and $t = 8$ [s].

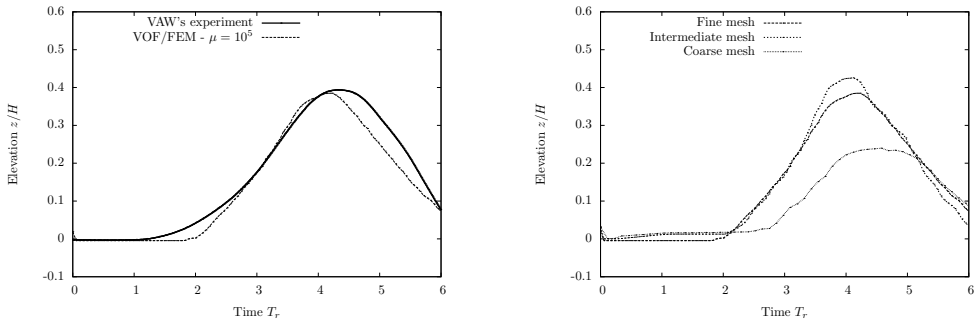

Figure 3: Wave generated by a landslide; free surface elevation at $x = 1.43$ m. Numerical results on the finest mesh. Left: Comparison between experimental data and numerical results with $\mu = 10^5$. Right: Grid convergence.

4.2 3D rigid bodies impact

We consider a rigid body falling into a water tank under the influence of gravity forces and initial conditions, that create a full three-dimensional wave that generalizes the im-

pulse waves simulation in pseudo-two-dimensional geometries from the previous section.

In the first example, we consider a rigid ball ($\rho = 2000$ [kg/m^3] , $\mu = 10^6$ [Pa s]) falling into a flat surface of water. The cavity dimensions are $2 \times 2 \times 10$ [m^3], while the ball is initially located at $(0, 0, 8)$ with radius 1.0 [m], and zero initial velocity. In this case, the capillary distance is approximately equal to 1 [cm], and thus surface tension effects are impossible to track with a reasonable mesh size and can be neglected. The water surface is located at height $z = 4$ [m]. The time step is 0.05 [s]. The results are illustrated in a cut in the middle of the computation domain. Figure 4 visualizes snapshots of the solid motion and the resulting, centrally located, impulse wave (or jet). The secondary droplets (the so-called wedding cake effect) are not tracked on this scale due to the mesh resolution.

Next we consider the same rigid body falling into two layers of liquid. The upper layer of fluid, located between $z = 2$ [m] and $z = 4$ [m], has density $\rho = 1000$ [kg/m^3] and viscosity $\mu = 10^{-2}$ [Pa s]. The lower layer of fluid, located below $z = 2$ [m], has density $\rho = 2000$ [kg/m^3] and viscosity $\mu = 10$ [Pa s]. Since the second layer of fluid is as dense as the rigid body, the rigid ball is going through both layers and eventually stabilizes in an equilibrium state that is approximately at the same height as the second layer of fluid (although this equilibrium position is not well-known from the modeling point of view to the best of our knowledge) (see Figure 5 for an illustration)

Finally we consider the same setup with two layers of fluid. However we consider a lower layer of fluid, located below $z = 2$ [m], with density $\rho = 3000$ [kg/m^3] and viscosity $\mu = 1$ [Pa s]. Since the second layer of fluid is more dense than the rigid body, the rigid ball does not go through the bottom layer. Figure 6 shows how the ball ends up between the two fluids in an equilibrium state in which the materials are ordered from the smallest to the highest density. Still a jet appears due do the reaction of the lighter fluid on top.

5 CONCLUSIONS

We have presented a numerical model for the density-dependent incompressible Navier-Stokes equations based on a VOF formulation. This model allows for the numerical simulation of multiphase flows involving an arbitrary number of immiscible liquid phases, together with a vacuum phase separated with a free surface. The numerical algorithm is based on an operator splitting strategy and a two-grid method. Numerical results have been presented for impulse waves (i) to validate the method with one example having experimental data available, and (ii) to show the efficiency of a model based on incompressible liquids for the numerical simulation of three-dimensional rigid bodies interacting with liquids.

ACKNOWLEDGMENTS

This work is partially funded by the Commission for technology and innovation CTI (grant number 14359.1 PFES-ES) and by the Swiss national science foundation project

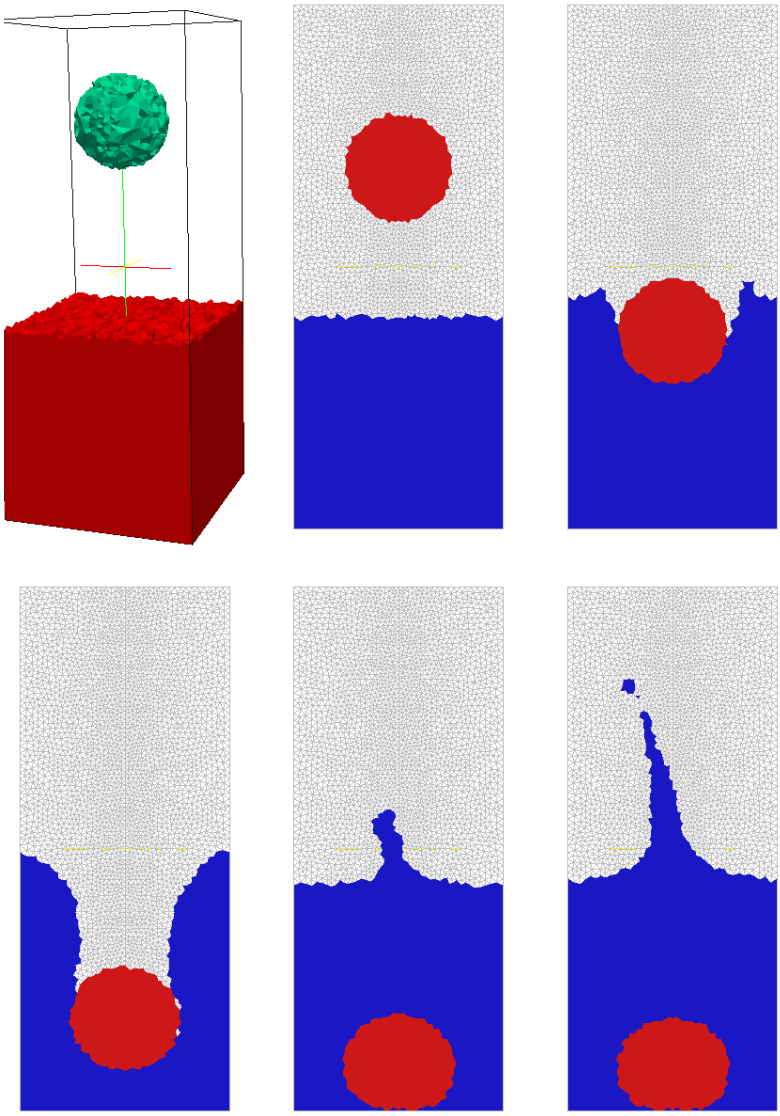

Figure 4: Nearly rigid ball falling into a water tank. Snapshots of the solution at times $t = 0$ [s] (three-dimensional view) and $t = 0.5, 1, 1.5, 2$ and 2.5 [s] (view along a vertical cut in the middle of the computational domain). Visualization of the ball location and wave propagation.

(grant number 200021_143470). This work has been initiated while S. Boyaval was a MATHICSE-ASN chair academic host; We thank Prof. W. W. Hager, Laboratory of Hydraulics, Hydrology and Glaciology (VAW, ETHZ), V. Laurmaa, J.-C. Makuch (EPFL), and A. Masserey and G. Steiner (Ycoor Systems SA) for fruitful discussions. All the computations have been performed with the EPFL cfsFlow software commercialized by Ycoor Systems SA.

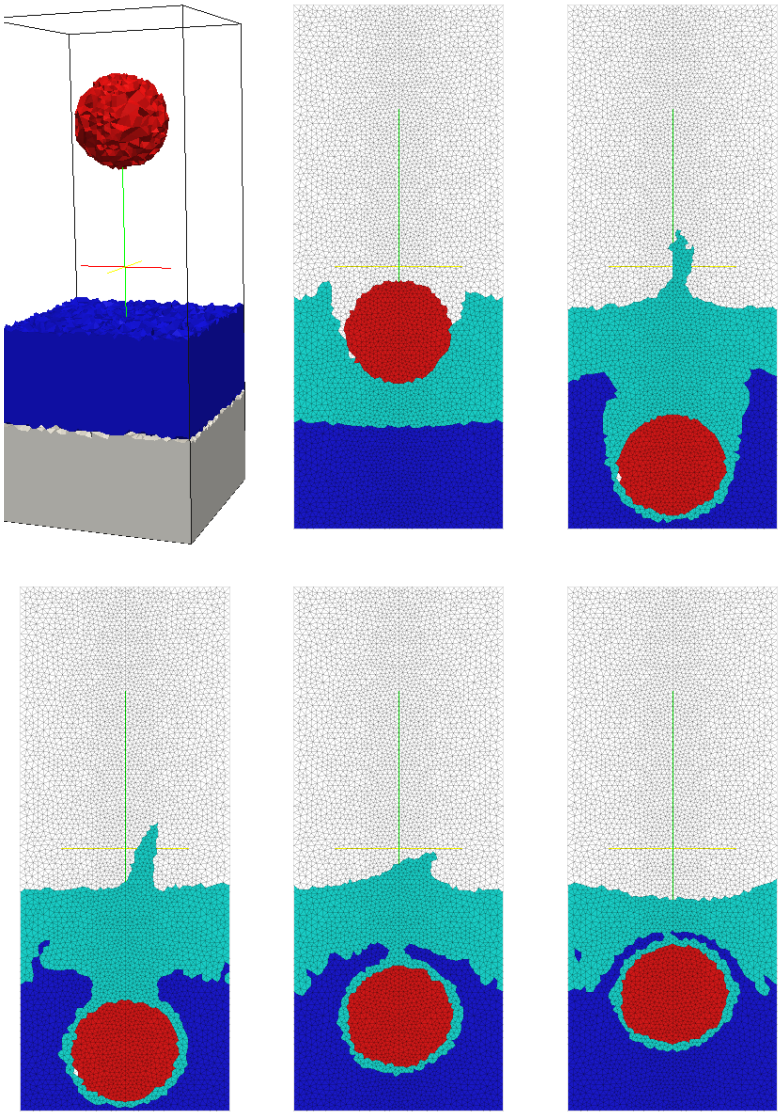

Figure 5: Rigid ball falling into a water tank with two layers of two liquids (bottom: light fluid). Snapshots of the solution at times $t = 0$ [s] (three-dimensional view) and $t = 1, 2, 3, 4$ and 5 [s] (view along a vertical cut in the middle of the computational domain). Visualization of the ball location and wave propagation.

REFERENCES

[1] H. T. Ahn and M. Shashkov. Multi-material interface reconstruction on generalized polyhedral meshes. *J. Comput. Phys.*, 226(2):2096–2132, 2007.

[2] A. Caboussat, M. Picasso, and J. Rappaz. Numerical simulation of free surface incom-

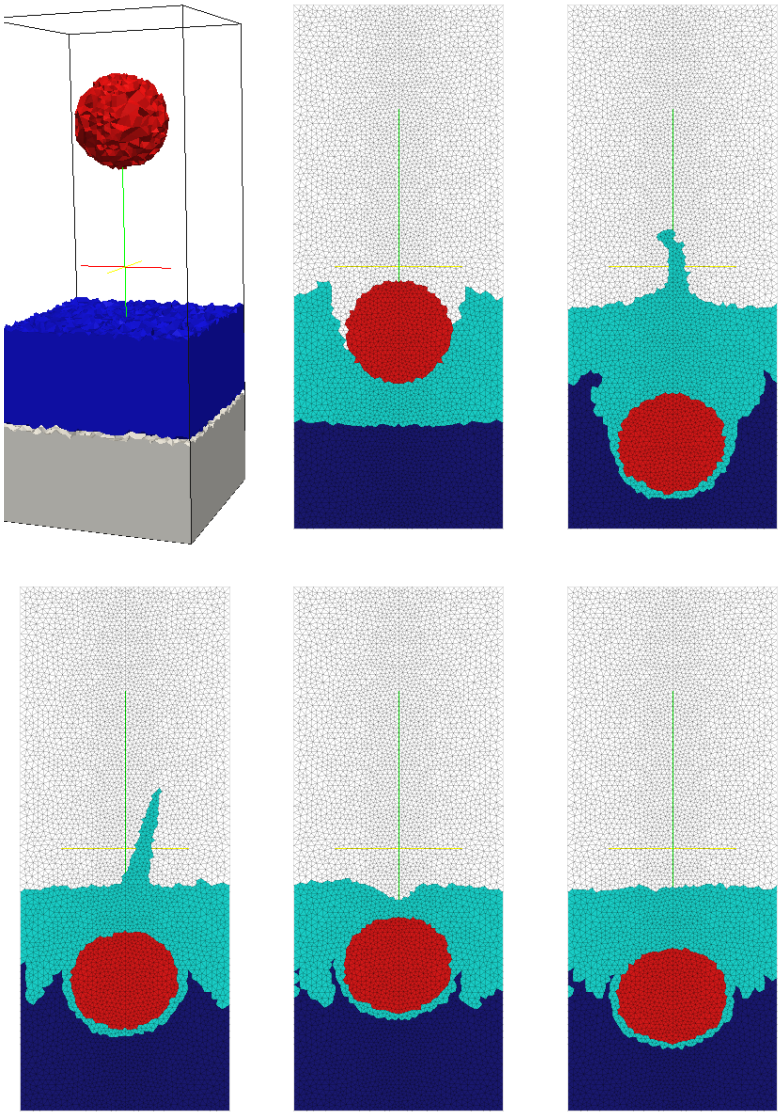

Figure 6: Rigid ball falling into a water tank with two layers of two liquids (bottom: dense fluid). Snapshots of the solution at times $t = 0$ [s] (three-dimensional view) and $t = 1, 2, 3, 4$ and 5 [s] (view along a vertical cut in the middle of the computational domain). Visualization of the ball location and wave propagation.

pressible liquid flows surrounded by compressible gas. *J. Comput. Phys.*, 203(2):626–649, 2005.

[3] B. Y. Choi and M. Bussmann. A piecewise linear approach to volume tracking a triple point. *Int. J. Numer. Methods Fluids*, 53(6):1005–1018, 2007.

[4] V. Dyadechko and M. Shashkov. Reconstruction of multi-material interfaces from moment data. *J. Comput. Phys.*, 227(11):5361–5384, 2008.

[5] L. P. Franca and S. L. Frey. Stabilized finite element methods: II. the incompressible Navier-Stokes equations. *Comp. Meth. Appl. Mech. Engrg*, 99(2-3):209–233, 1992.

[6] R. Glowinski. *Finite Element Method For Incompressible Viscous Flow*, volume IX of *Handbook of Numerical Analysis (P.G. Ciarlet, J.L. Lions eds)*, pages 3–1176. Elsevier, Amsterdam, 2003.

[7] V. Heller and W. H. Hager. Impulse product parameter in landslide generated impulse waves. *Journal of Waterway, Port, Coastal, and Ocean Engineering*, 136:145–155, 2010.

[8] N. James, S. Boyaval, A. Caboussat, and M. Picasso. Numerical simulation of 3d free surface flows: the case of multiple incompressible liquid phases. *Int. J. Numer. Meth. Fluids*, submitted, 2014.

[9] V. Maronnier, M. Picasso, and J. Rappaz. Numerical simulation of three-dimensional free surface flows. *Int. J. Numer. Meth. Fluids*, 42(7):697–716, 2003.

[10] S. P. Schofield, M. A. Christon, V. Dyadechko, R. V. Garimella, R. B. Lowrie, and B. K. Swartz. Multi-material incompressible flow simulation using the moment-of-fluid method. *Int. J. Numer. Meth. Fluids*, 63(8):931–952, 2010.

[11] A. Serrano-Pacheco, J. Murillo, and P. Garcia-Navarro. A finite volume method for the simulation of the waves generated by landslides. *Journal of Hydrology*, 373(3-4):273–289, 2009.

[12] M. Sussman. A second order coupled level set and volume-of-fluid method for computing growth and collapse of vapor bubbles. *J. Comput. Phys.*, 187(1):110–136, 2003.

[13] G. Tryggvason, R. Scardovelli, and S. Zaleski. *Direct numerical simulations of gas-liquid multiphase flows*. Cambridge University Press, Cambridge, 2011.

[14] Noh W.F. and Woodward Paul. SLIC (simple line interface calculation). *Proceedings of the Fifth International Conference on Numerical Methods in Fluid Dynamics*, 59:330–340, 1976.